NJC

PAPER

View Article Online
View Journal | View Issue

Cite this: *New J. Chem.*, 2019, 43, 12375

Synthesis and photophysical, thermal and antimycobacterial properties of novel 6-amino-2-alkyl(aryl/heteroaryl)-4-(trifluoromethyl) quinolines†

Yuri G. Kappenberg,[a] Alex Ketzer,[a] Felipe S. Stefanello,[a] Paulo R. S. Salbego,[a] Thiago V. Acunha,[b] Bruno L. Abbadi,[c] Cristiano V. Bizarro,[c] Luiz A. Basso,[c] Pablo Machado,[c] Marcos A. P. Martins,[a] Nilo Zanatta,[a] Bernardo A. Iglesias[b] and Helio G. Bonacorso*[a]

Received 1st April 2019,
Accepted 15th July 2019

DOI: 10.1039/c9nj01681c

rsc.li/njc

The synthesis and structural elucidation of a new series of six 6-amino-2-alkyl(aryl/heteroaryl)-4-(trifluoromethyl) quinolines are reported, yielding 22 to 87% isolated products. This was achieved through a regioselective intramolecular cyclization reaction of novel (*Z*)-4-((4-aminophenyl)amino)-1,1,1-trifluoro-but-3-en-2-ones in an acidic solvent-free medium, in which alkyl/aryl/heteroaryl = methyl, phenyl, 4-MeC_6H_4, 4-FC_6H_4, 4-$NO_2C_6H_4$, and 2-furyl. The novel compounds were fully characterized by ^{1}H-, ^{13}C- and ^{19}F-NMR spectroscopy, GC-MS and single-crystal X-ray diffraction. In addition, the preliminary investigation of photophysical properties of the 6-aminoquinolines (UV-Vis, fluorescence, quantum yield calculations, Stokes shifts, and TD-DFT analysis) and inhibitory activity against *M. tuberculosis* H37Rv strain was also presented. Thermal analyses were carried out to assess their properties as new materials.

Introduction

Quinoline derivatives are widely exploited because of their great biological applicability.[1] Studies have been undertaken to obtain new quinolines that can be used against malaria, for example, mefloquine (*Lariam*®), analogous to quinine (a natural antimalarial compound), whose consumption has been increasing. This compound has two trifluoromethyl groups (CF_3) in its structure and has presented a great efficiency against the parasite *Plasmodium falciparum*, the one responsible for human malaria.[2,3]

On the other hand, the CF_3 group is a very important substituent in medicinal, materials and agricultural chemistry,[4] due to its stereoelectronic properties, high lipophilicity, and resistance to enzyme degradation.[5–7] For this reason, its introduction into bioactive molecules has become very important in pharmaceutical studies.[8] In addition, it is reported that the amino group associated with quinolines has several biological applications, such as cell marking,[9] anticancer activity,[10] antimalarial activity,[11,12] antimycobacterial activity,[13] and antibacterial activity.[14] Considering the antitubercular activity, quinoline-containing compounds have been obtained as a scaffold of clinically useful anti-TB drugs such as bedaquiline[15] and fluoroquinolones.[16]

In recent years, the synthesis and fluorescent properties of a series of 6-aminoquinolines were reported.[17–22] As an example, this kind of molecule has shown luminescent properties, with potential applications in organic solar cells (OSCs), biomolecular markers, organic light-emitting diodes (OLEDs), molecular probes and switches.[17,19] Application of 6-aminoquinolines in photoluminescent sensors to detect different metals in solution has also been highlighted. This is possible through complex formation between quinoline with chelating groups attached and these species,[19–21] which leads to high quantum yield results and easier detection of these metal species in living organisms.[22]

Therefore, considering the importance of the studies involving aminoquinolines containing the trifluoromethyl substituent and alkyl(aryl/heteroaryl) substituents – which are rarely reported together – our research group decided to perform the synthesis of a series of 6-amino-2-alkyl(aryl/heteroaryl)-4-(trifluoromethyl)quinolines, and evaluate their photophysical and thermal properties, allied with an antimycobacterial evaluation.

[a] *Núcleo de Química de Heterociclos (NUQUIMHE), Departamento de Química, Universidade Federal de Santa Maria, 97105-900 Santa Maria, Brazil. E-mail: helio.bonacorso@ufsm.br*
[b] *Laboratório de Bioinorgânica e Materiais Porfirínicos, Departamento de Química, Universidade Federal de Santa Maria, Santa Maria, RS, 97105-900, Brazil*
[c] *Instituto Nacional de Ciência e Tecnologia em Tuberculose (INCT-TB), Centro de Pesquisas em Biologia Molecular e Funcional, Pontifícia Universidade Católica do Rio Grande do Sul, 90619-900 Porto Alegre, RS, Brazil*

† Electronic supplementary information (ESI) available: NMR spectra, crystallographic data, DSC curves, and UV-vis electronic absorption and emission fluorescence spectral data. CCDC 1895628 (**3b**) and 1895629 (**4d**). For ESI and crystallographic data in CIF or other electronic format see DOI: 10.1039/c9nj01681c

Results and discussion

Synthesis

The synthetic route and the structures of the 6-amino-4-(trifluoromethyl)quinolines are demonstrated in Scheme 1. Specific details of the experimental procedures and complete data for structural characterization are described in the ESI.† Firstly, a series of six examples of 4-methoxy-4-alkyl(aryl)-1,1,1-trifluoroalk-3-en-2-ones **1a–f** was synthesized from the trifluoroacetylation reactions of enol ethers or the respective acetals with trifluoroacetic anhydride in the presence of pyridine, in accordance with a methodology that has already been described.[23–25]

Subsequently, to obtain a novel series of (*Z*)-4-((4-aminophenyl)-amino)-1,1,1-trifluoroalk-3-en-2-ones **4a–f**, the reaction involving the enone **1b** and 1,4-phenylenediamine **2** was initially selected to find the best reaction conditions to obtain compounds **3a–f**. The temperature and solvent were evaluated using an equimolar ratio of both reactants. The reactions were carried out at 0 °C since the enone **1b** was still observed at room temperature. A decrease in the yield of **3b** was observed when the reaction solvent was changed from methanol (87%) to ethanol (82%), chloroform (73%), dichloromethane (71%) and acetonitrile (71%). In this sense, the best reaction conditions were adding **1b** dropwise to **2**, in pure methanol at 0 °C during 2 h. Under these conditions, it was possible to obtain a series of six new examples of enamino ketones (**3a–f**) yielding 71 to 87% isolated products.

The new structures (**3a–f**) were confirmed and characterized by ^{1}H-, ^{13}C-, ^{19}F-NMR and GC-MS techniques. The structural assignments for **3a–f** are consistent with the spectral data described in the literature for similar compounds.[26–30] The *E*-isomers can be distinguished from the *Z*-isomers by the ^{1}H-NMR spectra, because the N–H signals of the *E*-form (in 4–8 ppm) appear at a much higher magnetic field than those of the *Z*-form (in 9–13 ppm), indicating the presence of an intramolecular hydrogen interaction. The ^{1}H-NMR chemical shift of the enamino hydrogens for **3a–f** was observed in the range of 3.44 to 3.87 ppm, allowing one to assume that the enaminoketones **3a–f** exist in the *Z*-form in $CDCl_3$, which is stabilized by an intramolecular N–H···O=C interaction.[31] The ^{19}F-NMR spectra (in $CDCl_3$) of compounds **3a–f** showed only one singlet with an average value of −76.54 ppm corresponding to the CF_3 group. Additionally, single-crystal X-ray diffraction (SC-XRD) was performed for compound **3b** to confirm its molecular structure (Fig. S1, ESI†). This analysis corroborated the NMR data, showing the *Z*-form in the crystalline state for compound **3b**.

Table 1 Optimization of the reaction conditions for the synthesis of quinoline **4b**[a]

Entry	Acid	Acid[b] (mL)	Temperature (°C)	Time (h)	Yield **4b**[c] (%)
1	PPA	1.2 : 0.8	90	2	—[d]
2	PPA	1.2 : 0.8	90	6	7
3	PPA	1.2 : 0.8	120	2	41
4	PPA	1.2 : 0.8	120	6	48
5	PPA	1.2 : 0.8	120	10	21
6	PPA	1.2 : 0.8	165	2	17
7	PPA	1.2 : 0.8	120	6	23
8	H_2SO_4	5	90	2	—[d]
9	H_2SO_4	5	120	2	47
10	H_2SO_4	5	150	2	37
11	H_2SO_4	5	120	6	57
12	H_2SO_4	5	120	10	61
13	H_2SO_4	5	120	24	50
14	H_2SO_4	7	120	10	59
15	H_2SO_4	3	120	10	56

[a] For all entries: **3b** (1.0 mmol). [b] For PPA: P_2O_5 (1.2 g): H_3PO_4 (0.8 mL). [c] Isolated yield. [d] Mixture of starting material **3b** and traces of product **4b**.

Subsequently, the enaminoketones **3** were employed in the synthesis of the respective 6-amino-4-(trifluoromethyl)quinolines **4a–f**. The enamino ketone **3b** was used to perform the optimization of the reaction conditions. The intramolecular cyclization reaction was carried out in the presence of a strongly acidic solvent-free medium, in accordance with previously described methodologies.[32–34]

Compound **3b** was added to polyphosphoric acid–PPA (P_2O_5 + H_3PO_4), and the reaction time and temperature were varied (Table 1 – entries 1–7). The progress of all reactions was monitored by TLC. Unfortunately, tests using PPA medium were not satisfactory, leading to the degradation of products at high temperatures and very low yields at low temperatures. In a second strategy, the reaction was performed using concentrated sulfuric acid, varying the same parameters as in the PPA case (Table 1 – entries 8–15). Finally, the best reaction conditions were observed using a solution of **3b** (1.0 mmol) with concentrated sulfuric acid (5 mL) at 120 °C for 10 h (Table 1 – entry 12). Under these conditions, the desired 6-aminoquinolines **4a–f** were obtained yielding 22 to 87% isolated products (Table 2).

The structures of 6-aminoquinolines **4a–f** were characterized by ^{1}H-, ^{13}C-, and ^{19}F-NMR spectroscopy and GC-MS techniques, and also compared with reported data of similar compounds.[22,35–37] It is reported that the synthesis of quinolines can lead to a mixture of two types of isomers (2-CF_3 and 4-CF_3) when the reaction involves the use of anilines with 1,3-dicarbonyl compounds in acid medium.[38,39] However, our research group recently reported

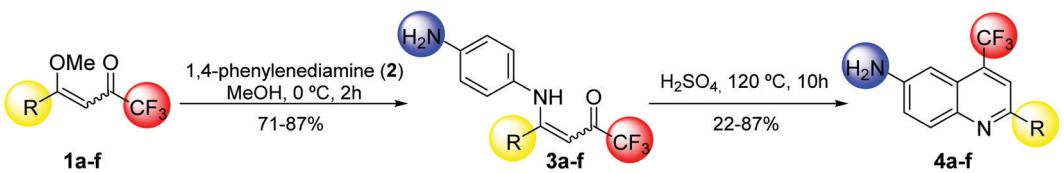

R = Me (**a**), C_6H_5 (**b**), 4-MeC_6H_4 (**c**), 4-FC_6H_4 (**d**), 4-$NO_2C_6H_4$ (**e**), 2-furyl (**f**).

Scheme 1 Synthesis of 6-amino-4-(trifluoromethyl)quinolines **4**.

Table 2 Intramolecular cyclocondensation reaction for 2-alkyl(aryl/heteroaryl)-6-amino-4-(trifluoromethyl)quinolines (**4a–f**)[a,b]

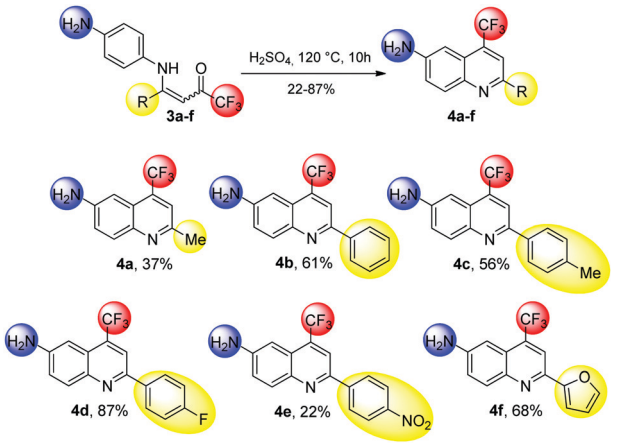

[a] Reaction conditions: H_2SO_4 conc. (5 mL), enaminoketones **3a–f** (1 mmol), 120 °C, 10 h. [b] Isolated yields.

a successful regioselective intramolecular cyclization reaction that enabled the isolation of the 4-CF_3 isomer.[40]

The chemical shifts for the 2-CF_3 isomer showed quartets at 122.3 ppm ($^1J_{CF}$ = 275 Hz) for the CF_3 group and at 148.5 ppm ($^2J_{CF}$ = 34 Hz) for C-2; whereas, the 4-CF_3 isomer showed quartets at 124.2 ppm ($^1J_{CF}$ = 275 Hz) for the CF_3 group and at 134.8 ppm ($^2J_{CF}$ = 31 Hz) for C-4. In accordance with the data already described,[26,41,42] it was possible to confirm that the 6-aminoquinoline systems discussed herein present the trifluoromethyl group attached to 4-carbon. This, due to the chemical shifts obtained for the CF_3 group and C-4, was shown in the range of 123.9 ppm and 131.8 ppm, respectively.

It was possible to confirm the formation of compounds due to a long-range coupling with the fluorine atoms of the 4-trifluoromethyl substituent, and the H-5, which is represented as a quartet, but in some cases, the signal appears at a low resolution, as is well known in similar aromatic nitrogenated heterocycles. The ^{1}H NMR chemical shifts showed the proton of the NH_2 group bonded to C-6 as a singlet in the range of 4.07–6.39 ppm. The ^{19}F NMR spectra for compounds **4a–f** showed a singlet with an average value of −61.53 ppm representing the CF_3 group.

In order to confirm the molecular structure of 6-aminoquinolines **4a–f**, in the solid state, SC-XRD was carried out for compound **4d** (Fig. 1). The structure crystallized in the $P2_1/c$ space group. It was possible to verify that the dihedral angle between the substituent (4-FC_6H_4) and the quinoline ring (N1–C2–C21–C26) was 25.6°, which showed some degree of planarity of the molecule. Additional crystallographic data can be found in the ESI.†

General absorption and emission properties of compounds 4a–f

Absorption UV-Vis spectra[43,44] of the related compounds in three different solvents furnished peaks in the ultraviolet and

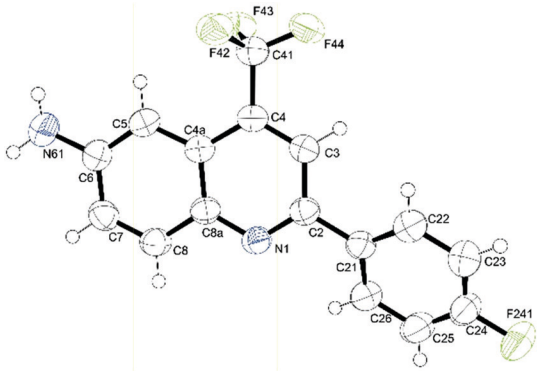

Fig. 1 ORTEP diagram of compound **4d**. Displacement ellipsoids are drawn at the 50% probability level.

visible region, around the 250–450 nm range (Fig. 2a and Table 3). In general, the first transition band observed is attributed to a $\pi \rightarrow \pi^*$ intraligand transition of the aromatic system. In the 300–350 nm range, broad bands are attributed to the $n \rightarrow \pi^*$ transition of electrons located on the quinoline structure.[45]

Bands located in the range of 350–450 nm can be assigned to the possible intermolecular charge transfer transition (ICT).[46] Small shifts in the lower energy transitions are observed for all derivatives, according to the solvent properties. Compound **4b** has a bathochromic shift in more polar solvents (DMSO and MeOH), as shown in Fig. 2a. These data are corroborated by TD-DFT calculation analysis (Table 4), in which the same tendency is observed. UV-Vis spectra of all compounds in different solvents are presented in the ESI† (Fig. S2–S6).

Emission fluorescence analysis demonstrated that all compounds showed fluorescence (purple to blue region) with good quantum fluorescence yield values (Φ_{fl}), in several solvents in the range of 400–700 nm. An influence of solvent in the Φ_{fl} values was observed. Compounds **4b** and **4d** presented higher Φ_{fl} values in $CHCl_3$, **4c** and **4b** in DMSO and **4d** and **4c** in MeOH (Table 3).

Moderate to higher Stokes shift values (38 to 102 nm range) were observed, and this can be assigned to the presence of the terminal amino group and the aryl-substituted moiety, when compared to the aromatic phenyl-quinoline derivatives.[44] The Stokes shifts data observed in all compounds can be attributed to the ICT transitions and electron-substituent properties that exist in these molecules, respectively. Emission fluorescence spectra of all derivatives in different solvents are presented in the ESI† (Fig. S7–S11).

It is interesting to insert a brief comparison related to the photophysical properties of compounds **4a–f** and other similar compounds already reported by our research group.[41,42] Compounds **4a–f** presented a more pronounced fluorescence quantum yield when compared with the morpholinyl and pyrrolidinyl-quinoline derivatives,[41] but smaller than the indolyl unit containing compounds.[42] This fact can be attributed to the presence of the indolyl moiety (high electronic conjugation) that favors the increase of Φ_{fl}. Moreover, the Stokes shift variation for **4a–f** (primary amines) (Fig. 2) is greater than the

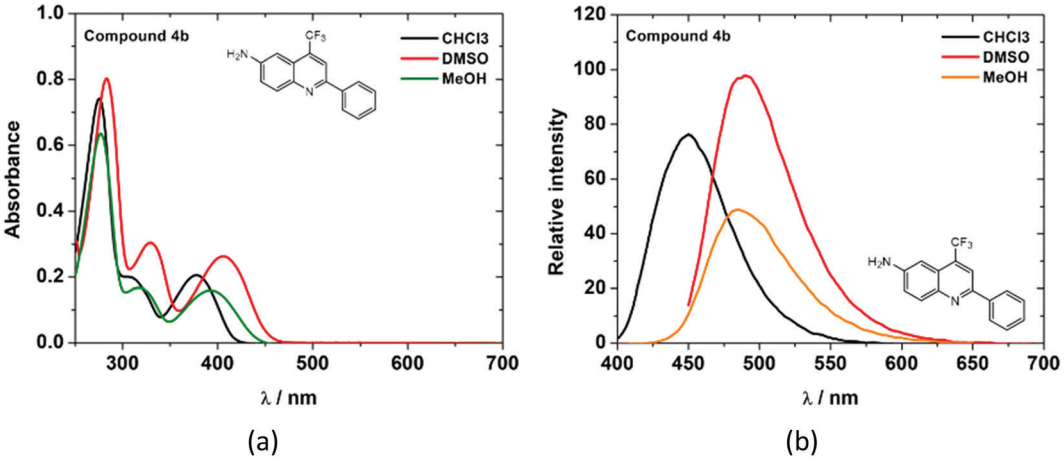

Fig. 2 (a) UV-vis spectra of compound **4b** in $CHCl_3$ (black line), DMSO (red line) and MeOH (green line), respectively. (b) Steady-state emission fluorescence spectra of compound **4b** in $CHCl_3$ (black line; λ_{exc} = 378 nm), DMSO (red line; λ_{exc} = 404 nm) and MeOH (orange line; λ_{exc} = 392 nm), respectively.

Table 3 Photophysical data of compounds **4a–f** in different solvents

Solvent	Compound	λ, nm (ε; M^{-1} cm^{-1})[a]	λ_{em} (Φ_f)[b]	SS[c] (nm)
$CHCl_3$	**4a**	252 (4310), 288 (sh), 366 (695)	448 (0.160)	82.0
	4b	275 (3705), 310 (990), 378 (1030)	449 (0.309)	71.0
	4c	279 (3600), 311 (1320), 380 (1220)	450 (0.220)	70.0
	4d	276 (3825), 309 (1040), 380 (1035)	454 (0.310)	74.0
	4e	270 (3075), 305 (2105), 349 (3145)	451 (0.268)	102.0
	4f	271 (2970), 299 (3610), 392 (1765)	457 (0.295)	65.0
DMSO	**4a**	258 (4495), 294 (820), 391 (785)	482 (0.336)	91.0
	4b	283 (4020), 329 (1525), 406 (1315)	489 (0.449)	83.0
	4c	284 (3885), 329 (1685), 407 (1370)	489 (0.466)	82.0
	4d	282 (3260), 329 (1215), 408 (1050)	488 (0.441)	80.0
	4e	281 (3495), 318 (sh), 431 (3355)	469 (0.375)	38.0
	4f	277 (2090), 305 (2610), 418 (1345)	496 (0.264)	78.0
MeOH	**4a**	252 (3235), 294 (390), 382 (450)	483 (0.117)	101.0
	4b	277 (3170), 320 (835), 393 (795)	485 (0.187)	92.0
	4c	280 (3435), 322 (1045), 394 (960)	487 (0.230)	93.0
	4d	277 (3050), 317 (800), 394 (735)	486 (0.265)	92.0
	4e	274 (3755), 304 (2205), 411 (3205)	495 (0.215)	84.0
	4f	271 (3270), 301 (4220), 405 (1870)	492 (0.010)	87.0

sh = shoulder. [a] Concentration = 2.0×10^{-4} M. [b] Concentration = 1.0×10^{-6} M, using DPA as standard (Φ_f = 0.65), in $CHCl_3$. [c] SS = Stoke shifts = $\Delta\lambda = \lambda_{em} - \lambda_{abs}$ (in nm).

Table 4 Excitation energy (E), wavelength of maximum absorbance (λ_{max}), and oscillator strength (f) for HOMO–LUMO orbitals in $CHCl_3$, DMSO and MeOH for compound **4b**

Solvent	E (eV)	λ_{max} (nm)	f
$CHCl_3$	3.238	382.93	0.2805
DMSO	3.213	385.92	0.2761
MeOH	3.222	384.78	0.2613

previously reported results for the respective tertiary amines (morpholinyl-, pyrrolidinyl- and indolyl-quinolines).

TD-DFT calculations of compounds 4a–f

For a better insight into the frontier orbitals of **4a–f**, DFT calculations were performed for these compounds using the Gaussian 09 package program.[47] A bathochromic shift in more polar solvents (DMSO and MeOH) was observed (Table 4), and these data are corroborated by the absorption and emission analyses.

Additionally, it was observed that the HOMO and LUMO density is uniformly distributed throughout the molecule, where small displacements at the lower energy transitions are observed (Table 5). It was also possible to observe that among the compounds obtained in this series, compound **4e** presented the most delocalized LUMO in the substituent (R = 4-$NO_2C_6H_4$) (Table 5).

Thermal analyses

Thermal analyses were carried out for compounds **4a–f** to furnish information regarding the stability and thermal behavior of this

Table 5 Energy and HOMO–LUMO density plots for **4a–f**, in $CHCl_3$

Compound	HOMO	LUMO	Energy (eV)
4a	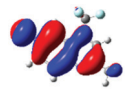	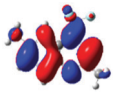	3.429
4b	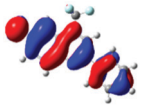	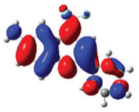	3.238
4c	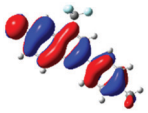	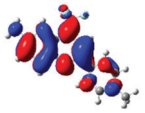	3.215
4d	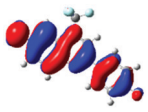	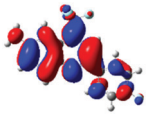	3.220
4e	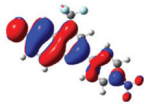	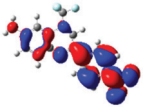	2.746
4f	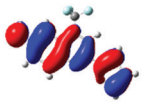	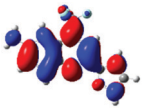	3.138

kind of structure. Understanding the thermal behavior is an important part of developing stable drugs and new materials. Thermogravimetric analysis (TGA) indicated that for all compounds (**4a–f**), decomposition occur in one major step (Fig. 3), ranging from around 145 to 280 °C (>95% decomposition) (Table 6).

The temperature of maximum decomposition (T_d), which corresponds to the temperature of the maximum peak in the derivative weight (%) as a function of temperature (T), ranged from 176 to 270 °C (Fig. 3 and Table 6). This information demonstrates that the compounds **4a–f** present a high decomposition temperature, allowing their use in applications that require this condition. The aryl compounds (**4b–e**) presented

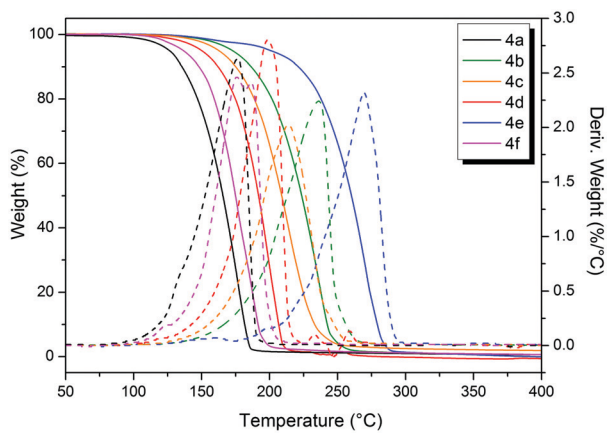

Fig. 3 Thermogravimetric analysis for compounds **4a–f**.

Table 6 Thermal analyses data (DSC and TGA) of compounds **4a–f**

	Compound					
Thermal data[a]	**4a**	**4b**	**4c**	**4d**	**4e**	**4f**
T_m[b] (°C)	—[h]	121.4	99.0	138.0	—[h]	—[h]
ΔH_m[c] (kJ mol^{-1})	—[h]	3.9	3.0	6.8	—[h]	—[h]
T_c[d] (°C)	—[h]	—[h]	—[h]	69.0	—[h]	—[h]
ΔH_c[e] (kJ mol^{-1})	—[h]	—[h]	—[h]	5.4	—[h]	—[h]
T_{onset}[f] (°C)	145.3	200.7	185.9	175.1	237.9	155.8
T_{endset}[f] (°C)	184.5	245.7	233.2	209.0	2813	194.0
T_d[g] (°C)	176.8	236.1	214.2	198.4	269.5	175.9

[a] All DSC data are given from the first heating–cooling cycle. [b] Melting temperature. [c] Melting enthalpy. [d] Temperature of crystallization. [e] Crystallization enthalpy. [f] Data from TGA. [g] Temperature of maximum decomposition obtained by TGA. [h] No thermal event detected in the studied temperature range.

higher thermal stability when compared with compounds **4a** and **4f**, in which both presented similar values of T_d. Compound **4e** presented the higher thermal stability (T_d of 269 °C), starting its decomposition above 200 °C and ending close to 300 °C.

Compounds **4a–f** were submitted for DSC analysis (Fig. S18–S23, ESI†) in order to determine their thermal events (*e.g.*, melting and crystallization temperatures). The compounds were subjected to three cycles of heating and cooling in a safe temperature range varied according to their decomposition temperature. This was done to avoid decomposition within the DSC equipment. Melting events were observed only in compounds **4b–d**, with melting enthalpies of 3.9, 3.0 and 6.8 kcal mol^{-1}, respectively (Table 6 and Fig. S19–S21, ESI†). Compound **4d** also presented a crystallization event at 69 °C with an enthalpy of 5.4 kcal mol^{-1} (Table 6 and Fig. S21, ESI†). No thermal event was detected in any of the three heating–cooling cycles, in the studied temperature range, for compounds **4a**, **4e** and **4f** (Table 6 and Fig. S18, S22, S23, ESI†). These data demonstrate that these compounds (**4a**, **4e** and **4f**) can be used in applications that require a solid state at high temperatures (150–238 °C).

Antimycobacterial evaluation

The synthesized compounds **4a–f** were evaluated in a whole-cell assay against *M. tuberculosis* strain H37Rv using isoniazid (INH) as the standard drug.[48] The 6-amino-4-(trifluoromethyl)quinolines **4b** and **4c** showed moderate activity against the bacillus under the evaluated conditions (Table 7). Considering the data shown, one can conclude that, in general, aryl substituents exhibited better activity than the alkyl (**4a**) and heteroaryl groups (**4f**). The most active compounds **4b** and **4c** inhibited the *M. tuberculosis* growth with MIC values of 69.2 μM and 66.0 μM, respectively. These compounds have phenyl and *p*-tolyl groups attached at the 2-position of the quinoline ring. Interestingly, exchanging the methyl group at the 4-position of the benzene (**4c**) with a fluoro atom generated a molecule of reduced activity as compound **4d** was ineffective at the highest concentration tested. This preliminary SAR finding demonstrates that steric and electronic properties of substituents attached at the 2-position of the heterocyclic compounds appear to be linked to their antimycobacterial activities. However, more studies are

Table 7 Activity of 6-amino-2-alkyl(aryl/heteroaryl)-4-(trifluoromethyl)-quinolines **4a–f** against *Mycobacterium tuberculosis* H37Rv strain

Compound	MIC[a] (μM)
4a	>88.1
4b	69.2
4c	66.0
4d	>65.1
4e	—
4f	71.7
INH	2.3

[a] The MIC value reported here for each compound was the most frequent value observed in three independent experiments. Compound **4e** showed low solubility under the assay conditions. INH, isoniazid.

needed to clarify this point. In addition, the molecular prediction about toxicological risks of **4b** and **4c** was obtained using the OSIRIS-Property-Explorer (Actelion Pharmaceuticals Ltd, Allschwil, Switzerland). Results of the toxicity risk predictor showed that the compounds may not present risk of irritating and reproductive effects. Additionally, the compounds may present a medium risk for mutagenicity and tumorigenicity. These results suggest a possible low toxicity of the compounds and a likely high degree of selectivity for *M. tuberculosis.*

Conclusions

In summary, it was possible to obtain and fully characterize a new series of six 6-amino-2-alkyl(aryl/heteroaryl)-4-(trifluoromethyl)quinolines. The compounds were obtained at yields of 22–87% from a regioselective intramolecular cyclization reaction. This study shows the possibility of further studies using this kind of synthetic approach to obtain aminoquinolines containing trifluoromethyl and alkyl(aryl/heteroaryl) substituents. Preliminary investigations showed promising photophysical properties and high thermal stability of the obtained aminoquinolines. Finally, the antimycobacterial activity elicited by the 6-amino-2-alkyl(aryl/heteroaryl)-4-(trifluoromethyl)quinolines suggests that this class of compounds may furnish molecules for the future development of anti-TB drugs.

Experimental section

Unless otherwise indicated, all common reagents and solvents were used as obtained from commercial suppliers, without further purification. ^{1}H and ^{13}C NMR spectra were acquired on a Bruker DPX 400 MHz spectrometer for one-dimensional experiments and on a Bruker Avance III 600 MHz for ^{19}F NMR spectra and 2D-experiments (gHMBC). 5 mm sample tubes were used, at 298 K, with a digital resolution of ±0.01 ppm, in $CDCl_3$, using TMS as the internal reference. All results were reported as follows: chemical shift (δ) (multiplicity, integration, coupling constant). The following abbreviations were used to explain multiplicities: s = singlet, bs = broad singlet, d = doublet, t = triplet, q = quartet, qui = quintet, m = multiplet, dd = doublet of doublets. All NMR chemical shifts were reported in parts per million relative to the internal reference (TMS).

Melting points of compounds **3a–f** were determined using coverslips on a Microquímica MQAPF-302 apparatus. High-resolution mass spectra (HRMS) were obtained for all compounds on an LTQ Orbitrap Discovery mass spectrometer (Thermo Fisher Scientific). This hybrid system combines the LTQ XL linear ion trap mass spectrometer and an Orbitrap mass analyzer. The experiments were performed *via* direct infusion of the sample (flow: 10 μL min^{-1}) in positive-ion mode using electrospray ionization. Elemental composition calculations for comparison were executed using the specific tool included in the Qual Browser module of Xcalibur (Thermo Fisher Scientific, release 2.0.7) software.

Single crystals of compounds **3b** and **4d** were obtained by slow evaporation of EtOH/H_2O and $CHCl_3$, respectively, at 25 °C. Diffraction measurement of compound **3b** was performed using a Bruker D8 Venture with a Photon 100 CMOS detector with graphite monochromatized Mo Kα radiation (λ = 0.71073 Å). Compound **4d** was measured using a Bruker D8 QUEST diffractometer using Cu Kα radiation (λ = 1.54080 Å) with a KAPPA four-circle goniometer equipped with a PHOTON II CPAD area detector. Absorption corrections were performed using the multi-scan method. Anisotropic displacement parameters for non-hydrogen atoms were applied. Most hydrogen atom positions were calculated geometrically and refined using the riding model, but some hydrogen atoms were refined freely. The structure was solved and refined using the WinGX software package.[49] The structures were refined based on the full-matrix least-squares method using the SHELXL program.[50] The ORTEP projections of the molecular structures were generated using the ORTEP-3 program.[49] Crystallographic information files (CIFs) for the novel structures were deposited at the Cambridge Crystallographic Data Centre (CCDC) under identification number 1895628 (**3b**) and 1895629 (**4d**). Crystallographic data can be observed in the ESI† (Fig. S1 and Table S2).

UV-vis absorption spectra were recorded using a Shimadzu UV-2600 spectrophotometer (data interval, 1.0 nm) using $CHCl_3$, DMSO or MeOH as solvent, using a concentration of 2.0×10^{-4} M for each compound. Fluorescence spectra of samples in all solutions were measured with a Varian Cary50 fluorescence spectrophotometer (emission; slit 1.0 mm) and were corrected according to the manufacturer's instructions. The lowest energy electronic transition of each derivative to be excited (emission spectrum) was chosen. Fluorescence quantum yield (Φ_f) values of the related compounds in solutions were determined by comparing the corrected fluorescence spectra with that of 9,10-diphenylanthracene (DPA) in chloroform (Φ_f = 0.65, λ_{ex} = 366 nm) as the standard fluorescence yield.

All calculations were carried out using the Gaussian 09 package of programs.[47] All geometrical structures were optimized at the SCRF(PCM)-B3LYP/cc-pVTZ level of theory, with single-point energies and molecular orbitals calculated at the same level of theory. The PCM model was used to account for the solvent effect. Harmonic frequency calculations were carried out in order to confirm that the geometries were at the minimum potential energy.

The thermal events (melting and crystallization temperatures and associated enthalpies) of compounds **4a–f** were determined

using differential scanning calorimetry (DSC) with an MDSC Q2000 (T-zeroTM DSC technology, TA Instruments Inc., USA). Dry high purity (99.999%) nitrogen gas was used as the purge gas (50 mL min^{-1}). Samples were crimped in hermetic aluminum pans with lids. The heating rate used for all the samples was 5 °C min^{-1}. The samples were submitted to three heating–cooling cycles, with a temperature range of −80 °C to the beginning of the decomposition temperature of each compound, observed by thermogravimetric analysis (TGA). The TGA was performed on a TGA Q5000 (TA Instruments Inc., USA). The heating rate used was 10 °C min^{-1} in an inert atmosphere of N_2 (50 mL min^{-1}). The DSC sample was weighed on a Sartorius scale (M500P) with an accuracy of ±0.001 mg. Data were obtained using TA Universal Analysis 2000 Software, version 4.5 (TA Instruments Inc., USA).

The minimum inhibitory concentration (MIC) of the compounds **4a–f** was evaluated by the resazurin reduction microplate assay (REMA) in *M. tuberculosis* H37Rv (ATCC 27294) strain, as previously described.[47] The compounds (**4a–d** and **4f**) were first solubilized in neat dimethyl sulfoxide (DMSO – Sigma-Aldrich) at a concentration of 4 mg mL^{-1}, and then diluted to a concentration of 40 μg mL^{-1} in Middlebrook 7H9 broth (Becton Dickinson – BD Difco), supplemented with 10% ADC enrichment (albumin, dextrose, and catalase – BD Difco) and 5% DMSO (7H9-ADC broth). Compound **4e** was insoluble in 7H9-ADC broth, thus its MIC value was not determined. Compounds were twofold serially diluted in 7H9-ADC broth in 96-well U-bottom polystyrene microtiter plates, providing a concentration range of 20–0.04 μg mL^{-1}. Bacterial growth control (without antibiotic) and compound sterility control (without culture) were included in each test. Mycobacterial suspensions were prepared from log-phase cultures (OD_{600} 0.6–0.8) grown in 7H9-ADC broth with 0.05% Tween 80 (Sigma-Aldrich). Cells were vortexed with sterile beads (1 mm) for 3 minutes and then allowed to rest for 20 min at room temperature. The suspension was spectrophotometrically measured (OD_{600}) and aliquots were stored at −20 °C. Frozen cell aliquots were thawed and diluted to a theoretical OD of 0.006 ($\approx 1 \times 10^6$ CFU mL^{-1}) in 7H9-ADC broth and 100 μL was added to each well (final volume = 200 μL). Plates were sealed with parafilm and incubated inside plastic bags in a humidity chamber for 7 days (37 °C, 5% CO_2). Then, 60 μL of a fresh filter-sterilized 0.01% (wt/vol) resazurin (Sigma-Aldrich) solution was added and plates were additionally incubated for 48 h. Mycobacterial growth was visually indicated by the reduction of the blue-colored resazurin into the pink-colored resorufin and MIC was considered as the lowest drug concentration that prevented this color change. Three independent experiments were performed, and the MIC value reported was the most frequent value observed among the three assays, or the highest value obtained when there was a discrepancy between the assays.

General procedure for synthesis of (*Z*)-4-((aminophenyl)-amino)-1,1,1-trifluorobut-3-en-2-ones (3a–f)

To a magnetically stirred solution of 1,4-phenylenediamine (**2**) (1 mmol, 0.108 g) in methanol (10 mL), a solution of 4-methoxy-1,1,1-trifluorobut-3-en-2-ones (**3a–f**) (1 mmol) in methanol (10 mL) was added dropwise at 0 °C over a period of 2 h. After the end of the reaction, traces of the solvent were evaporated under reduced pressure and the products **3a–f** recrystallized from ethanol and water. The solution was then cooled to −10 °C, and yellow, red or brown solids were obtained. The solids were filtered under reduced pressure, washed with cold water, and dried under reduced pressure.

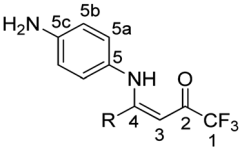

(*Z*)-4-((4-Aminophenyl)amino)-1,1,1-trifluoropent-3-en-2-one (3a). Physical aspect: yellow solid. Yield: 71%. Melting point: 78–80 °C. ^{1}H NMR (400 MHz, $CDCl_3$) δ: 12.41 (s, 1H, NH), 6.97–6.89 (m, 2H, H-5a), 6.69–6.64 (m, 2H, H-5b), 5.48 (s, 1H, H-3), 3.80 (s, 2H, NH_2), 2.04 (s, 3H, Me). ^{13}C NMR (100 MHz, $CDCl_3$) δ: 175.82 (q, J = 32.9 Hz, C-2), 168.84 (C-4), 146.04 (C-5c), 127.55 (C-5), 126.54 (C-5a), 117.69 (q, J = 288.2 Hz, CF_3), 115.32 (C-5b), 90.24 (C-3), 20.14 (Me). ^{19}F NMR (565 MHz, $CDCl_3$) δ: −76.59 (CF_3). GC-MS (EI, 70 eV): m/z (%): 244 (M^+, 100), 175 (85). HRMS (ESI): (M + H^+): calc. for $C_{11}H_{11}F_3N_2O$: 245.0896. Found: 245.0914.

(*Z*)-4-((4-Aminophenyl)amino)-1,1,1-trifluoro-4-phenylbut-3-en-2-one (3b). Physical aspect: yellow solid. Yield: 87%. Melting point: 124–126 °C. ^{1}H NMR (400 MHz, $CDCl_3$) δ: 12.56 (s, 1H, NH), 7.44–7.38 (m, 1H, C_6H_5), 7.37–7.31 (m, 4H, C_6H_5), 6.69–6.64 (m, 2H, H-5a), 6.53–6.49 (m, 2H, H-5b), 5.67 (d, J = 0.6 Hz, 1H, H-3), 3.44 (s, 2H, NH_2). ^{13}C NMR (100 MHz, $CDCl_3$) δ: 176.72 (q, J = 33.3 Hz, C-2), 166.65 (C-4), 144.82 (C-5c), 134.16 (C_6H_5), 130.40 (C_6H_5), 128.74 (C_6H_5), 128.65 (C-5), 128.3 (C_6H_5), 125.49 (C-5a), 117.60 (q, J = 288.2 Hz, CF_3), 115.20 (C-5b), 91.78 (C-3). ^{19}F NMR (565 MHz, $CDCl_3$) δ: −76.49 (CF_3). GC-MS (EI, 70 eV): m/z (%): 306 (M^+, 100), 238 (17), 237 (99), 203 (16). HRMS (ESI): (M + H^+): calc. for $C_{16}H_{13}F_3N_2O$: 307.1053. Found: 307.1075.

(*Z*)-4-((4-Aminophenyl)amino)-1,1,1-trifluoro-4-(*p*-tolyl)but-3-en-2-one (3c). Physical aspect: yellow solid. Yield: 75%. Melting point: 134–136 °C. ^{1}H NMR (400 MHz, $CDCl_3$) δ: 12.54 (s, 1H, NH), 7.22–7.16 (m, 2H, 4-MeC_6H_4), 7.15–7.06 (m, 2H, 4-MeC_6H_4), 6.71–6.61 (m, 2H, H-5a), 6.52–6.41 (m, 2H, H-5b), 5.62 (d, J = 0.6 Hz, 1H, H-3), 3.46 (s, 2H, NH_2), 2.34 (s, 3H, Me). ^{13}C NMR (150 MHz, $CDCl_3$) δ: 176.53 (q, J = 33.0 Hz, C-2), 166.77 (C-4), 144.71 (C-5c), 140.88 (4-MeC_6H_4), 131.19 (4-MeC_6H_4), 129.31 (C-5), 128.98 (4-MeC_6H_4), 128.36 (4-MeC_6H_4), 125.47 (C-5a), 117.65 (q, J = 288.3 Hz, CF_3), 115.21 (C-5b), 91.65 (C-3), 21.42 (Me). ^{19}F NMR (565 MHz, $CDCl_3$) δ: −76.47 (CF_3). GC-MS (EI, 70 eV): m/z (%): 320 (97), 251 (100), 203 (26). HRMS (ESI): (M + H^+): calc. for $C_{17}H_{15}F_3N_2O$: 321.1209. Found: 321.1231.

(*Z*)-4-((4-Aminophenyl)amino)-1,1,1-trifluoro-4-(4-fluorophenyl)but-3-en-2-one (3d). Physical aspect: yellow solid. Yield: 76%. Melting point: 107–110 °C. ^{1}H NMR (400 MHz, $CDCl_3$) δ: 12.49 (s, 1H, NH), 7.36–7.30 (m, 2H, 4-FC_6H_4), 7.07–7.00 (m, 2H, 4-FC_6H_4), 6.70–6.65 (m, 2H, H-5a), 6.61–6.57 (m, 2H, H-5b), 5.65 (d, J = 0.6 Hz, 1H, H-3), 3.87 (s, 2H, NH_2).

^{13}C NMR (150 MHz, $CDCl_3$) δ: 176.89 (q, J = 33.4 Hz, C-2), 165.55 (C-4), 163.72 (d, J = 252.1 Hz, 4-FC_6H_4), 144.84 (C-5c), 130.62 (d, J = 8.8 Hz, 4-FC_6H_4), 130.16 (d, J = 3.9 Hz, 4-FC_6H_4), 128.60 (C-5), 125.61 (C-5a), 117.52 (q, J = 288.4 Hz, CF_3), 115.91 (d, J = 22.0 Hz, 4-FC_6H_4), 115.32 (C-5b), 91.70 (C-3). ^{19}F NMR (565 MHz, $CDCl_3$) δ: −76.53 (CF_3), −108.73 (4-FC_6H_4). GC-MS (EI, 70 eV): m/z (%): 324 (M^+, 100), 256 (15), 255 (88), 203 (16). HRMS (ESI): (M + H^+): calc. for $C_{16}H_{12}F_4N_2O$: 325.0959. Found: 325.0981.

(*Z*)-4-((4-Aminophenyl)amino)-1,1,1-trifluoro-4-(4-nitrophenyl)-but-3-en-2-one (3e). Physical aspect: red solid. Yield: 85%. Melting point: 156–159 °C. ^{1}H NMR (400 MHz, $CDCl_3$) δ: 12.41 (s, 1H, NH), 8.23–8.11 (m, 2H, 4-$NO_2C_6H_4$), 7.57–7.46 (m, 2H, 4-$NO_2C_6H_4$), 6.67–6.62 (m, 2H, H-5a), 6.54–6.46 (m, 2H, H-5b), 5.66 (s, 1H, H-3), 3.74 (s, 2H, NH_2). ^{13}C NMR (100 MHz, $CDCl_3$) δ: 177.69 (q, J = 33.9 Hz, C-2), 163.84 (C-4), 148.56 (4-NO-C_6H_4), 145.39 (C-5c), 140.56 (4-$NO_2C_6H_4$), 129.57 (4-$NO_2C_6H_4$), 127.84 (C-5), 125.80 (4-$NO_2C_6H_4$), 123.82 (C-5a), 117.23 (q, J = 288.7 Hz, CF_3), 115.31 (C-5b), 91.88 (C-3). ^{19}F NMR (565 MHz, $CDCl_3$) δ: −76.66 (CF_3). GC-MS (EI, 70 eV): m/z (%): 353 (M^+, 100), 282 (22), 236 (71), 235 (25). HRMS (ESI): (M + H^+): calc. for $C_{16}H_{12}F_3N_3O_3$: 352.0904. Found: 352.0930.

(*Z*)-4-((4-Aminophenyl)amino)-1,1,1-trifluoro-4-(furan-2-yl)but-3-en-2-one (3f). Physical aspect: brown solid. Yield 86%. Melting point: 107–109 °C. ^{1}H NMR (400 MHz, $CDCl_3$) δ: 12.35 (s, 1H, NH), 7.47 (dd, J = 1.8, 0.7 Hz, 1H, 2-furyl), 6.96–6.90 (m, 2H, H-5a), 6.68–6.64 (m, 2H, H-5b), 6.35 (dd, J = 3.6, 1.7 Hz, 1H, 2-furyl), 6.14 (dd, J = 3.7, 0.7 Hz, 1H, 2-furyl), 6.12 (s, 1H, H-3), 3.78 (s, 2H, NH_2). ^{13}C NMR (100 MHz, $CDCl_3$) δ: 176.96 (q, J = 33.3 Hz, C-2), 155.54 (C-4), 146.16 (2-furyl), 145.78 (2-furyl), 145.22 (C-5c), 128.96 (C-5), 126.89 (C-5a), 117.69 (q, J = 288.0 Hz, CF_3), 117.49 (2-furyl), 115.48 (C-5b), 112.32 (2-furyl), 87.16 (C-3). ^{19}F NMR (565 MHz, $CDCl_3$) δ: −76.51 (CF_3). GC-MS (EI, 70 eV): m/z (%): 296 (M^+, 100), 279 (32), 227 (26). HRMS (ESI): (M + H^+): calc. for $C_{14}H_{11}F_3N_2O_2$: 297.0845. Found: 297.0987.

General procedure for synthesis of 2-alkyl(aryl/heteroaryl)-6-amino-4-(trifluormethyl)quinolines (4a–f)

To a flask containing 1 mmol of (*Z*)-4-((4-aminophenyl)amino)-1,1,1-trifluoroalk-3-en-2-ones (**3a–f**), 5 mL of concentrated sulfuric acid was added. The reaction mixture was heated at 120 °C under magnetic stirring for 10 h. After cooling the system to room temperature, the reaction mixture was treated with distilled water (5 mL) and was neutralized with a solution of saturated $NaHCO_3$. The compounds **4a–f** were extracted with ethyl acetate (3 × 20 mL) and the organic phase was dried with Na_2SO_4, filtered, and then the solvent was removed under reduced pressure. The products **4a–f** were purified by column chromatography on silica gel using hexane as eluent.

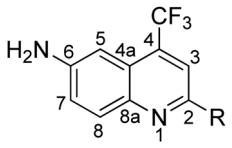

2-Methyl-4-(trifluoromethyl)quinolin-6-amine (4a). Physical aspect: yellow solid. Yield: 37%. Melting point: not observed; decomposition around 145 °C. ^{1}H NMR (400 MHz, $CDCl_3$) δ: 7.90 (dd, J = 9.0, 0.5 Hz, 1H, H-8), 7.46 (s, 1H, H-3), 7.18 (dd, J = 9.0, 2.5 Hz, 1H, H-7), 7.13 (qui, J = 2.2 Hz, 1H, H-5), 4.07 (s, 2H, NH_2), 2.71 (s, 3H, Me). ^{13}C NMR (100 MHz, $CDCl_3$) δ: 153.85 (C-2), 145.29 (C-6), 143.96 (C-8a), 131.93 (q, J = 31.1 Hz, C-4), 130.74 (C-8), 123.79 (q, J = 274.3 Hz, CF_3), 122.92 (C-4a), 121.90 (C-7), 119.20 (q, J = 5.4 Hz, C-3), 103.83 (d, J = 2.2 Hz, C-5), 24.81 (Me). ^{19}F NMR (565 MHz, $CDCl_3$) δ: −62.46 (CF_3). GC-MS (EI, 70 eV): m/z (%): 226 (100), 198 (M^+, 6), 157 (6). HRMS (ESI): (M + H^+): calc. for $C_{11}H_9F_3N_2$: 227.0791. Found: 227.0807.

2-Phenyl-4-(trifluoromethyl)quinolin-6-amine (4b). Physical aspect: yellow solid. Yield: 61%. Melting point: 121 °C. ^{1}H NMR (600 MHz, $CDCl_3$) δ: 8.11 (d, J = 7.3 Hz, 2H, C_6H_5), 8.07–8.03 (m, 2H, H-3, H-8), 7.51 (m, 2H, C_6H_5), 7.44 (t, J = 7.3 Hz, 1H, C_6H_5), 7.21 (dd, J = 9.0, 2.5 Hz, 1H, H-7), 7.16 (qui, J = 2.2 Hz, 1H, H-5), 4.15 (s, 2H, NH_2). ^{13}C NMR (150 MHz, $CDCl_3$) δ: 152.58 (C-2), 145.89 (C-6), 144.33 (C-8a), 138.84 (C_6H_5), 132.28 (q, J = 31.2 Hz, C-4), 131.90 (C-8), 129.27 (C_6H_5), 128.93 (C_6H_5), 127.02 (C_6H_5), 123.91 (q, J = 274.4 Hz, CF_3), 123.69 (C-4a), 122.19 (C-7), 116.30 (q, J = 5.3 Hz, C-3), 103.55 (C-5). ^{19}F NMR (565 MHz, $CDCl_3$) δ: −62.39 (CF_3). GC-MS (EI, 70 eV): m/z (%): 288 (100), 289 (M^+, 19), 287 (13), 219 (11). HRMS (ESI): (M + H^+): calc. for $C_{16}H_{11}F_3N_2$: 289.0947. Found: 289.0968.

2-(*p*-Tolyl)-4-(trifluoromethyl)quinolin-6-amine (4c). Physical aspect: orange solid. Yield: 56%. Melting point: 99 °C. ^{1}H NMR (400 MHz, $CDCl_3$) δ: 8.06–7.97 (m, 4H, H-3, H-8, 4-MeC_6H_4), 7.30 (d, J = 7.9 Hz, 2H, 4-MeC_6H_4), 7.18 (dd, J = 9.0, 2.5 Hz, 1H, H-7), 7.14 (qui, J = 2.2 Hz, 1H, H-5), 4.14 (s, 2H, NH_2), 2.41 (s, 3H, Me). ^{13}C NMR (100 MHz, $CDCl_3$) δ: 152.60 (C-2), 145.77 (C-6), 144.31 (C-8a), 139.39 (4-MeC_6H_4), 136.05 (4-MeC_6H_4), 132.21 (q, J = 31.0 Hz, C-4), 131.77 (C-8), 129.67 (4-MeC_6H_4), 126.90 (4-MeC_6H_4), 123.98 (q, J = 274.4 Hz, CF_3), 123.56 (C-4a), 122.14 (C-7), 116.16 (q, J = 5.5 Hz, C-3), 103.63 (q, J = 2.1 Hz, C-5), 21.33 (Me). ^{19}F NMR (565 MHz, $CDCl_3$) δ: −62.40 (CF_3). GC-MS (EI, 70 eV): m/z (%): 302 (100), 303 (M^+, 19), 301 (19), 233 (6). HRMS (ESI): (M + H^+): calc. for $C_{17}H_{13}F_3N_2$: 303.1104. Found: 303.1126.

2-(4-Fluorophenyl)-4-(trifluoromethyl)quinolin-6-amine (4d). Physical aspect: pale yellow solid. Yield: 87%. Melting point: 138 °C. ^{1}H NMR (400 MHz, $CDCl_3$) δ: 8.16–8.11 (m, 2H, 4-FC_6H_4), 8.05 (dd, J = 9.0, 0.5 Hz, 1H, H-8), 8.02 (s, 1H, H-3), 7.27–7.17 (m, 4H, H-5, H-7, 4-FC_6H_4), 4.17 (s, 2H, NH_2). ^{13}C NMR (100 MHz, $CDCl_3$) δ: 163.73 (d, J = 248.8 Hz, 4-FC_6H_4), 151.46 (C-2), 145.92 (C-6), 144.31 (C-8a), 135.02 (d, J = 3.1 Hz, 4-FC_6H_4), 132.41 (q, J = 31.0 Hz, C-4), 131.84 (C-8), 128.82 (d, J = 8.2 Hz, 4-FC_6H_4), 123.87 (q, J = 274.3 Hz, CF_3), 123.60 (C-4a), 122.26 (C-7), 115.99–115.66 (m, C-3, 4-FC_6H_4), 103.53 (C-5). ^{19}F NMR (565 MHz, $CDCl_3$) δ: −62.43 (CF_3), −112.47 (4-FC_6H_4). GC-MS (EI, 70 eV): m/z (%): 306 (100), 307 (M^+, 18), 305 (9), 237 (9). HRMS (ESI): (M + H^+): calc. for $C_{16}H_{10}F_4N_2$: 307.0853. Found: 307.0875.

2-(4-Nitrophenyl)-4-(trifluoromethyl)quinolin-6-amine (4e). Physical aspect: yellow solid. Yield: 22%. Melting point: not observed; decomposition around 238 °C. ^{1}H NMR (600 MHz, DMSO-d_6) δ: 8.50 (d, J = 8.9, 2H, 4-$NO_2C_6H_4$), 8.35 (d, J = 8.9, 2H, 4-$NO_2C_6H_4$), 8.32 (s, 1H, H-3), 7.96 (d, J = 9.1 Hz, 1H, H-8), 7.36 (dd, J = 9.1, 2.3 Hz, 1H, H-7), 7.01 (bs, 1H, H-5), 6.39 (s, 2H,

NH_2). ^{13}C NMR (150 MHz, DMSO-d_6) δ: 149.86 (C-2), 147.37 (C-6), 146.59 (4-$NO_2C_6H_4$), 143.95 (C-8a), 142.57 (4-$NO_2C_6H_4$), 131.61 (C-8), 129.59 (q, J = 30.3 Hz, C-4), 127.44 (4-$NO_2C_6H_4$), 124.21 (C-4a), 123.88 (4-$NO_2C_6H_4$), 123.88 (q, J = 274.5 Hz, CF_3), 123.16 (C-7), 116.11 (q, J = 5.0 Hz, C-3), 99.57 (C-5). ^{19}F NMR (565 MHz, $CDCl_3$) δ: −56.94 (CF_3). GC-MS (EI, 70 eV): m/z (%): 333 (100), 334 (M^+, 19), 287 (41), 218 (14). HRMS (ESI): ($M + H^+$): calc. for $C_{16}H_{10}F_3N_3O_2$: 334.0798. Found: 334.0824.

2-(Furan-2-yl)-4-(trifluoromethyl)quinolin-6-amine (4f). Physical aspect: yellow solid. Yield: 68%. Melting point: not observed; decomposition at 156 °C. ^1H NMR (400 MHz, $CDCl_3$) δ: 8.03–7.96 (m, 2H, H-3, 2-furyl), 7.60 (dd, J = 1.8, 0.8 Hz, 1H, 2-furyl), 7.20 (dd, J = 9.0, 2.5 Hz, 1H, 2-furyl, H-7), 7.15 (dd, J = 3.4, 0.8 Hz, 1H, H-8), 7.13 (qui, J = 2.2 Hz, 1H, H-5), 6.58 (dd, J = 3.4, 1.7 Hz, 1H, 2-furyl), 4.16 (s, 2H, NH_2). ^{13}C NMR (100 MHz, $CDCl_3$) δ: 153.18 (C-2), 145.83 (C-6), 144.66 (C-8a), 144.02 (2-furyl), 143.88 (2-furyl), 132.19 (q, J = 31.5 Hz, C-4), 131.53 (C-8), 123.71 (q, J = 274.8 Hz, CF_3), 123.60 (C-4a), 122.29 (C-7), 115.15 (q, J = 5.6 Hz, C-3), 112.28 (2-furyl), 109.32 (2-furyl), 103.80 (C-5). ^{19}F NMR (565 MHz, $CDCl_3$) δ: −62.57 (CF_3). GC-MS (EI, 70 eV): m/z (%): 278 (100), 249 (11), 139 (7). HRMS (ESI): ($M + H^+$): calc. for $C_{14}H_9F_3N_2O$: 279.0740. Found: 279.0761.

Conflicts of interest

There are no conflicts to declare.

Acknowledgements

The authors acknowledge the Conselho Nacional de Desenvolvimento Científico e Tecnológico (CNPq) (CNPq/Universal, 402.075/2016-1), Fundação de Amparo à Pesquisa do Estado do Rio Grande do Sul (FAPERGS) (PqG, 17/2551-0001275-5; DOCFIX, 18/2551-0000562-2), and the National Institute of Science and Technology on Tuberculosis (Decit/SCTIE/MS-MCT-CNPq-FNDTC-CAPES-FAPERGS) (grant number 421703/2017-2) for the financial support. The fellowships from Coordenação de Aperfeiçoamento de Pessoal de Nível Superior (CAPES) (P. R. S. S., process number: 88887.197556/2018-00) are also acknowledged. The authors also acknowledge the SC-XRD team of the NUQUIMHE group, especially Tainára Orlando, for analyses and kind assistance.

References

1 O. Afzal, S. Kumar, M. R. Haider, M. R. Ali, R. Kumar, M. Jaggi and S. Bawa, *Eur. J. Med. Chem.*, 2015, **97**, 871–910.
2 G. C. Muscia, M. Bollini, J. P. Carnevale, A. M. Bruno and S. E. Asís, *Tetrahedron Lett.*, 2006, **47**(50), 8811–8815.
3 H. G. Bonacorso, S. H. G. Duarte, N. Zanatta and M. A. P. Martins, *Synthesis*, 2002, 1037–1042.
4 W. Zhu, J. Wang, S. Wang, Z. Gu, J. L. Aceña, K. Izawa, H. Liu and V. A. Soloshonok, *J. Fluorine Chem.*, 2014, **167**, 37–54.
5 B. E. Smart, *J. Fluorine Chem.*, 2001, **109**(1), 3–11.
6 R. D. Chambers, *Fluorine in Organic Chemistry*, Blackwell Oxford, UK, 2004.
7 J. P. Begué and D. Bonnet-Delpon, *Bioorganic and Medicinal Chemistry of Fluorine*, John Willey & Sons, Hoboken, NJ, 2008.
8 E. L. Luzina and A. V. Popov, *Eur. J. Med. Chem.*, 2012, **53**, 364–373.
9 N. Perin, L. Uzelac, I. Piantanida, G. Karminski-Zamola, M. Kralj and M. Hranjec, *Bioorg. Med. Chem.*, 2011, **19**(21), 6329–6339.
10 N. Wang, M. Świtalska, M. Y. Wu, K. Imai, T. A. Ngoc, C. Q. Pang, L. Wang, J. Wietrzyk and T. Inokuchi, *Eur. J. Med. Chem.*, 2014, **78**, 314–323.
11 K. J. Raynes, P. A. Stocks, P. M. O'Neill, B. K. Park and S. A. Ward, *J. Med. Chem.*, 1999, **42**(15), 2747–2751.
12 M. Jain, C. V. R. P. Reddy, M. Halder, S. Singh, R. Kumar, S. G. Wasudeo, P. P. Singh, S. I. Khan, M. R. Jacob, B. L. Tekwani and R. Jain, *ACS Omega*, 2018, **3**(3), 3060–3075.
13 J. Otevrel, P. Bobal, I. Zadrazilova, R. Govender, M. Pesko, S. Keltosova, P. Koleckarova, P. Marsalek, A. Imramovsky, A. Coffey, J. Mahony, P. Kollar, A. Cizek, K. Kralova and J. Jampilek, *Molecules*, 2013, **18**(9), 10648–10670.
14 S. M. Prajapati, K. D. Patel, R. H. Vekariya, S. N. Panchal and H. D. Patel, *RSC Adv.*, 2014, **4**(47), 24463–24476.
15 J. C. Palomino and A. Martin, *Future Microbiol.*, 2013, **8**(9), 1071–1080.
16 R. K. Shandil, R. Jayaram, P. Kaur, S. Gaonkar, B. L. Suresh, B. N. Mahesh, R. Jayashree, V. Nandi, S. Bharath and V. Balasubramanian, *Antimicrob. Agents Chemother.*, 2007, **51**(2), 576–582.
17 G. C. dos Santos, R. O. Servilha, E. F. de Oliveira, F. C. Lavarda, V. F. Ximenes and L. C. da Silva-Filho, *J. Fluoresc.*, 2017, **27**(5), 1709–1720.
18 T. Uchacz, P. Szlachcic, K. Wojtasik, M. Mac and K. Stadnicka, *Dyes Pigm.*, 2016, **124**, 277–292.
19 G. Pourfallah and X. Lou, *Dyes Pigm.*, 2018, **158**, 12–19.
20 G. J. Park, H. Kim, J. J. Lee, Y. S. Kim, S. Y. Lee, S. Lee, I. Noh and C. Kim, *Sens. Actuators, B*, 2015, **215**, 568–576.
21 K. Vongnam, T. Aree, M. Sukwattanasinitt and P. Rashatasakhon, *ChemistrySelect*, 2018, **3**(12), 3495–3499.
22 X. Meng, S. Wang, Y. Li, M. Zhu and Q. Guo, *Chem. Commun.*, 2012, **48**(35), 4196–4198.
23 M. A. P. Martins, W. Cunico, C. M. P. Pereira, A. P. Sinhorin, A. Flores, H. G. Bonacorso and N. Zanatta, *Curr. Org. Synth.*, 2004, **1**(4), 391–403.
24 G. M. Siqueira, A. F. C. Flores, G. Clar, N. Zanatta and M. A. P. Martins, *Quim. Nova*, 1994, **17**, 24–26.
25 M. Hojo, R. Masuda and E. Okada, *Synthesis*, 1986, 1013–1014.
26 H. G. Bonacorso, R. Andrighetto, N. Krüger, J. Navarini, A. F. C. Flores, M. A. P. Martins and N. Zanatta, *J. Heterocycl. Chem.*, 2013, **50**(S1), 193–199.
27 H. G. Bonacorso, R. Andrighetto, N. Krüger, M. A. P. Martins and N. Zanatta, *J. Braz. Chem. Soc.*, 2011, **22**(8), 1426–1438.
28 M. A. P. Martins, R. L. Peres, G. F. Fiss, F. A. Dimer, R. Mayer, C. P. Frizzo, M. R. B. Marzari, N. Zanatta and H. G. Bonacorso, *J. Braz. Chem. Soc.*, 2007, **18**, 1486–1491.

29 H. G. Bonacorso, R. V. Lourega, F. J. Righi, E. D. Deon, N. Zanatta and M. A. P. Martins, *J. Heterocycl. Chem.*, 2008, **45**(6), 1679–1686.
30 H. G. Bonacorso, A. P. Wentz, S. R. T. Bittencourt, L. M. L. Marques, N. Zanatta and M. A. P. Martins, *Synth. Commun.*, 2002, **32**(3), 335–341.
31 J. C. Zhuo, *Magn. Reson. Chem.*, 1997, **35**(1), 21–29.
32 H. G. Bonacorso, R. L. Drekener, I. R. Rodrigues, R. P. Vezzosi, M. B. Costa, M. A. P. Martins and N. Zanatta, *J. Fluorine Chem.*, 2005, **126**(9), 1384–1389.
33 H. G. Bonacorso, T. S. Moraes, N. Zanatta, M. A. P. Martins and A. F. C. Flores, *ARKIVOK*, 2008, **16**, 75–83.
34 H. G. Bonacorso, T. S. de Moraes, N. Zanatta and M. A. P. Martins, *Synth. Commun.*, 2009, **39**(20), 3677–3686.
35 T. Pérez-Ruiz, C. Martínez-Lozano, V. Tomás and J. Carpena, *J. Pharm. Biomed. Anal.*, 1996, **14**(11), 1505–1511.
36 C. Wiethan, S. Z. Franceschini, H. G. Bonacorso and M. Stradiotto, *Org. Biomol. Chem.*, 2016, **14**(37), 8721–8727.
37 H. G. Bonacorso, G. M. Dal Forno, C. Wiethan, A. Ketzer, N. Zanatta, C. P. Frizzo, M. A. P. Martins and M. Stradiotto, *RSC Adv.*, 2017, **7**(69), 43957–43964.
38 J. C. Sloop, C. L. Bumgardner and W. D. Loehle, *J. Fluorine Chem.*, 2002, **118**(1–2), 135–147.
39 O. Lefebvre, M. Marull and M. Schlosser, *Eur. J. Org. Chem.*, 2003, 2115–2121.
40 H. G. Bonacorso, M. B. Rodrigues, S. C. Feitosa, H. S. Coelho, S. H. Alves, J. T. Keller, W. C. Rosa, A. Ketzer, C. P. Frizzo, M. A. P. Martins and N. Zanatta, *J. Fluorine Chem.*, 2018, **205**, 49–57.
41 H. G. Bonacorso, M. B. Rodrigues, B. A. Iglesias, C. H. da Silveira, S. C. Feitosa, W. C. Rosa, M. A. P. Martins, C. P. Frizzo and N. Zanatta, *New J. Chem.*, 2018, **42**(12), 10024–10035.
42 M. B. Rodrigue, S. C. Feitosa, C. W. Wiethan, W. C. Rosa, C. H. Silveira, A. B. Pagliari, P. Martins, N. Zanatta, B. A. Iglesias and H. G. Bonacorso, *J. Fluorine Chem.*, 2019, **221**, 84–90.
43 B. L. Auras, S. L. Meller, M. P. da Silva, A. Neves, L. H. Z. Cocca, L. DeBoni, C. H. da Silveira and B. A. Iglesias, *Appl. Organomet. Chem.*, 2018, **32**(5), e4318.
44 G. Padilha, B. A. Iglesias, D. F. Back, T. S. Kaufman and C. C. Silveira, *ChemistrySelect*, 2017, **2**(3), 1297–1304.
45 T. R. Chen, R. H. Chien, A. Yeh and J. D. Chen, *J. Organomet. Chem.*, 2006, **691**(9), 1998–2004.
46 A. P. Kulkarni, P. T. Wu, T. W. Kwon and S. A. Jenekhe, *J. Phys. Chem. B*, 2005, **109**(42), 19584–19594.
47 M. J. Frisch, G. W. Trucks, H. B. Schlegel, G. E. Scuseria, M. A. Robb, J. R. Cheeseman, G. Scalmani, V. Barone, G. A. Petersson, H. Nakatsuji, X. Li, M. Caricato, A. Marenich, J. Bloino, B. G. Janesko, R. Gomperts, B. Mennucci, H. P. Hratchian, J. V. Ortiz, A. F. Izmaylov, J. L. Sonnenberg, D. Williams-Young, F. Ding, F. Lipparini, F. Egidi, J. Goings, B. Peng, A. Petrone, T. Henderson, D. Ranasinghe, V. G. Zakrzewski, J. Gao, N. Rega, G. Zheng,W. Liang, M. Hada, M. Ehara, K. Toyota, R. Fukuda, J. Hasegawa, M. Ishida, T. Nakajima, Y. Honda, O. Kitao, H. Nakai, T. Vreven, K. Throssell, J. A. Montgomery, Jr., J. E. Peralta, F. Ogliaro, M. Bearpark, J. J. Heyd, E. Brothers, K. N. Kudin, V. N. Staroverov, T. Keith, R. Kobayashi, J. Normand, K. Raghavachari, A. Rendell, J. C. Burant, S. S. Iyengar, J. Tomasi, M. Cossi, J. M. Millam, M. Klene, C. Adamo, R. Cammi, J. W. Ochterski, R. L. Martin, K. Morokuma, O. Farkas, J. B. Foresman and D. J. Fox, *Gaussian 09, Revision A.02*, Gaussian, Inc., Wallingford CT, 2016.
48 B. C. Giacobbo, K. Pissinate, V. Rodrigues-Junior, A. D. Villela, E. S. Grams, B. L. Abbadi, F. T. Subtil, N. Sperotto, R. V. Trindade, D. F. Back, M. M. Campos, L. A. Basso, P. Machado and D. S. Santos, *Eur. J. Med. Chem.*, 2017, **126**, 491–501.
49 L. J. Farrugia, WinGX and ORTEP for Windows: an update, *J. Appl. Crystallogr.*, 2012, **45**, 849–854.
50 G. M. A. Sheldrick, A short history of SHELX, *Acta Crystallogr., Sect. A: Found. Crystallogr.*, 2008, **64**, 112–122.

